Alma Mater Studiorum Università di Bologna
Archivio istituzionale della ricerca

Heterogeneous Multi-Rate mass transfer models in OPENFOAM®

(Article begins on next page)

22 November 2024

Heterogeneous Multi-Rate mass transfer models in OPENFOAM®

Federico **Municchi**[a], Nicodemo di **Pasquale**[a], Marco **Dentz**[b] and Matteo **Icardi**[a,*]

[a]*School of Mathematical Sciences, University of Nottingham, NG7 2RD, UK*
[b]*Institute of Environmental Assessment and Water Research (IDÆA-CSIC), Barcelona, Spain*

ABSTRACT

We implement the Multi-Rate Mass Transfer (MRMT) model for mobile-immobile transport in porous media [30, 43] within the open-source finite volume library OPENFOAM® [25]. Unlike other codes available in the literature [26, 58], we propose an implementation that can be applied to complex three-dimensional geometries and highly heterogeneous fields, where the parameters of the MRMT can arbitrarily vary in space. Furthermore, being built over the widely diffused OPENFOAM® library, it can be easily extended and included in other models, and run in parallel.We briefly describe the structure of the *multiContinuumModels* library that includes the formulation of the MRMT based on the works of Haggerty and Gorelick [30] and Municchi and Icardi [44]. The implementation is verified against benchmark solutions and tested on two- and three-dimensional random permeability fields. The role of various physical and numerical parameters, including the transfer rates, the heterogeneities, and the number of terms in the MRMT expansions, is investigated. Finally, we illustrate the significant role played by heterogeneity in the mass transfer when permeability and porosity are represented using Gaussian random fields.

1. Introduction

Interests in porous media dates back to the middle of nineteenth century with the study of Darcy describing the law that bears his name [66]. The reasons for such a long lasting interest reside in the fact that porous media are present in a wide range of systems and applications, both as natural [70] or industrial synthetic media. Also, environmental applications as risk and safety assessment of groundwater contamination [62, 61], reservoir storage, geothermal extraction, geological disposal of radioactive waste [51] and carbon dioxide require the study of fluid flow and solute transport in heterogeneous porous and fractured media.

One of the key characteristic of these systems is their heterogeneity, which results in non-equilibrium and memory effects [20, 16]. A porous medium can be described as a matrix of solid material in which a fluid phase moves. Usually, the region occupied by the fluid phase (mono or multi-component) is called *mobile* region whereas the remaining region, occupied by the matrix, is the *immobile* region. It is often assumed that the dominant transport process in the immobile regions is diffusion [44], while the mobile region can exchange mass and energy with the immobile region. Figure 1 depicts a typical domain composed of a mobile region and several immobile regions, similar to those often found in subsurface flow applications. Furthermore, such classification into mobile and immobile regions can be applied to fluid and fillers in packed beds or even to circulation and recirculation zones in fluid flows [69].

ORCID(s):

The complexity of flow fields into a highly heterogeneous medium (such as a porous medium) modify the transport behaviour of solutes within the fluid. In these kinds of systems non-Fickian transport behaviour is observed [52, 21]. The nature of the non-Fickian transport was extensively studied in literature [5, 7, 52], and its origin was found in the broad spectrum of transition times intrinsic to heterogeneous media [4].

Generally, immobile regions do not just introduce heterogeneities leading to non-Fickian dispersion in the porous medium, but they also act as storage (of heat or mass), leading to the breaking of time locality. As a result, the dynamics is non-local in time and therefore, it depends on the history of the system. Several methods were devised to mathematically describe such phenomenon in porous media. Among the spectrum of methodologies, we want to recall:

- The Dual-Porosity formulation [41], where the medium is modelled as two overlapping continua (mobile and immobile);

- The Integro-Differential formulation [32, 33, 12], which uses a mix of convolutions of state variables and memory functions to model non-local mass transfer;

- The Continuous Time Random Walk [6, 18, 4], which assumes a random walk in time and space for the movement of solute particles in a heterogeneous medium.

One of the formulations which received significant attention in the past decades is the Multi-Rate Mass Transfer (MRMT) Model [57, 30, 31, 65, 28, 3] which can be seen as a generalisation of the dual-porosity model. In the MRMT one performs a spectral decomposition of the diffusion operator in each immobile region, leading to infinite series of response terms representing the non-local transfer [44]. Thus, mass transfer between mobile and immobile regions is linear and can be represented by a suite of first-order processes or diffusive mass transfer processes. The interest in the MRMT model also stems from being mathematically equivalent to the other models described earlier [17, 58], while maintaining the important property of localisation. This means that the state of the heterogeneous systems can be described, at any instant of time, locally and without the need to define global quantities, which usually allow less flexibility in the description of these complex systems. Notice that in the MRMT model, a spectral decomposition is only performed in the immobile regions, which are often assumed to be simply connected and not complicated in shape. Therefore, the eigenfunctions can be easily obtained analytically in a large number of practical cases. However, the MRMT model does not apply to the mobile region, where the fluid is flowing. Therefore, macroscopic quantities like the effective fluxes must be obtained using other methods (for example, classical volume averaging [67] or two-scale asymptotics [45]). But this does not play a role in the numerical implementation of the MRMT model, which governs the inter-region transfer process.

A wide range problems can be addressed by the MRMT methodology, a fact that makes this framework extremely flexible and useful. An important environmental problem we are currently facing, is the high concentration of CO_2 in the atmosphere, due to anthropogenic contribution (mainly energy production). One of the most promising strategies devised to reduce carbon emissions is the Carbon Capture and Storage (CCS) through gas hydrate and crystallisation [60]. This process separates the CO_2 from fuel gas, by sequestration in gas hydrate crystals (mainly water). It was observed this process can be improved using porous media, thanks to their much high gas/water contact area [1]. Therefore, a reliable model for transport properties in such systems becomes essential.

Another environmental application is dispersion of contaminants in aquifer and groundwater remediation, where the dynamic of diffusion of chemical compounds into the ground is studied. One of the way to perform *in situ* remediation which has recently gained significant attention, involves the injection of a reactive suspension of engineered nanoparticles to degrade transform, or immobilise the pollutants[27, 68]. Both the dynamics of the dispersion of the pollutant, and the transport of these nanoparticles [40] are dominated by the exchanging of mass or energy with a set of impermeable inclusions, which could be modelled through MRMT.

A formulation of the numerical implementation of the MRMT model was presented in Silva et al. [58]. This approach is capable of describing a wide range of non-equilibrium phenomena by using a model which is local in time. Variables referring to immobile regions are solved as explicit functions, avoiding the need of a discretisation of these regions. By assuming a functional form for the the concentration in the mobile region during each time increment (in the [58] it was assumed a linear behaviour), it is possible to explicitly integrate the first-order linear differential equations referring to the immobile regions. Therefore, in this formulation the explicit contribution of each immobile region can be included in the discretised (in time and and space) equations describing the evolution of the concentration in the mobile region.
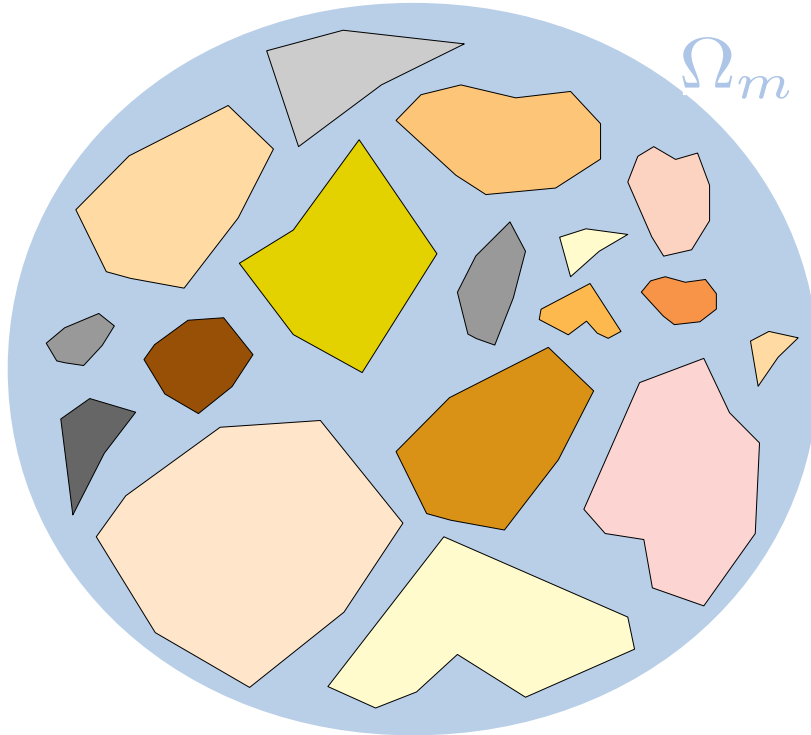
Figure 1: Representation of a typical heterogeneous medium with a mobile region (light blue) and several immobile regions (colours) with different shape and composition. Fluid is flowing in the mobile region only, while mass (or heat) can diffuse within the immobile regions.

In this work we propose a novel numerical implementation of the MRMT model, based on the generalisation proposed in an earlier work of some of the authors [44]. This numerical implementation is written as a new library within the C++ opensource finite volume library OpenFOAM® [50]. Our choice of OpenFOAM® was based on the fact that this code has a wide diffusion across industry and academia alike, and has a solid and active community of users.

This paper is structured as follows: we first present the relevant equations and hypothesis for the generalised MRMT model by following the derivation reported in [44]. We then proceed to show how these equations can be implemented in OpenFOAM® by describing the structure of the new library we are presenting and we report some examples of application of our library in a number of cases. We then proceed to draw some conclusions and outlooks on possible further uses of this library.

2. Mathematical formulation of the MRMT model

We present here the theoretical background of the MRMT model and we refer to [44] for a complete derivation of the relevant equations. However, notice that the notation we employ is slightly different from that used in [44], where the main focus was on the derivation of macroscopic equations from the microscale dynamics. The present work focuses on the macroscale exclusively and therefore, we will use primed symbols to indicate microscopic quantities and un-primed symbols to indicate macroscopic averaged quantities.

One point we want to emphasize here is that, while we are using the symbol c for the main quantities to be intended as a concentration of some chemical species in the domanin, the equations can be easily adapted to any other scalar quantity (such as the temperature). Our use of this terminology comes form the fact that this model comes from geological applications and we wanted to be consisted with the terminology used in this field.

Let us consider a heterogeneous domain Ω composed of a *mobile* region, Ω_m, and a number N of *immobile* regions, Ω_i, with $i = 1, \dots, N$ such that $\Omega = \Omega_m \bigcup_{i=1}^{N} \Omega_i$ (see Figure 1).

We assume the transport in the mobile region can be modelled by the advection-diffusion equation:

$$\frac{\partial c'_m}{\partial t} + \nabla \cdot \left(\boldsymbol{u}' c'_m - \mathcal{D}'_m \nabla c'_m \right) = 0, \quad \boldsymbol{x} \in \Omega_m. \tag{1}$$

where c'_m is a scalar field (which will be referred to as "concentration" for simplicity, even if it could be a temperature field as well), $\mathcal{D}'_m$ is the diffusion coefficient in the mobile region and $\boldsymbol{u}'$ is the velocity field. Furthermore, we consider N_i diffusion equations, one for each immobile region describing the concentrations $c'_i(\mathbf{x}, t)$ in the i-th immobile region:

$$\frac{\partial c'_i}{\partial t} = \mathcal{D}'_i \nabla^2 c'_i, \quad \boldsymbol{x} \in \Omega_i, \quad i = 1, \dots, N_i. \tag{2}$$

where $\mathcal{D}'_i$ is the diffusion coefficient in the i-th immobile region. Note that in previous equations we dropped the spatial and temporal dependence from c'_m and c'_i to simplify the notation. The equations describing the evolution of the concentration field in the mobile and the immobile regions must be coupled with the proper boundary conditions between the two kind of regions. Specifically, we impose continuity of fields and fluxes through the interfaces:

$$c'_i = c'_m, \quad \mathcal{D}'_i \frac{\partial c'_i}{\partial n} = \mathcal{D}'_m \frac{\partial c'_m}{\partial n}, \quad \boldsymbol{x} \in \partial\Omega_i. \tag{3}$$

An important implication of such boundary condition is that each immobile region is connected only to the mobile region, i.e. the immobile regions are not connected. Note that we consider here linear transport of a passive tracer. It is straightforward to account for linear equilibrium sorption in this modeling framework through retardation factors for the mobile and immobile domains as detailed in [30]. Chemical reactions in the mobile and immobile regions can be accounted for by the addition of source and sink terms in the conservation equations for the mobile and immobile species [e.g., 38, 39, 23, 19, 54]. Also non-linear relations between the scalar concentrations in the mobile and immobile zones can be modeled in this framework as done by [63] in the context of two-phase flow in fractured media.

The next step requires to smooth the concentration field by applying a suitable spatial filtering. In [44] two filters were defined: the volume filter over Ω and the Favre filter acting on the volume of the mobile region Ω_m. We will call $\overline{c}$ the volume averaged concentration field and c (instead of c') the Favre averaged concentration field. The relation between the two is [44]:

$$c_m = \frac{1}{V_m} \int_{\Omega_m} c'_m dV, \quad c_i = \frac{1}{V_i} \int_{\Omega_i} c'_i dV, \tag{4}$$

$$\overline{c}_m = \beta_m c_m, \quad \overline{c}_i = \beta_i c_i \tag{5}$$

which allows to write the concentration field in terms of a quantity (the Favre filtered concentration field) specific only to the mobile region. In the previous equation we also introduced the capacity of the mobile region, β_m, defined as the ratio between the volume of the region Ω, V, and the volume of the mobile region, V_m, so that $\beta_m = V/V_m$. Similarly, $\beta_i = V/V_i$, being V_i the volume occupied by the i-th immobile region.

By applying the volume filtering to eq. (1) and using eq. (3) and eq. (5) along with the Gauss-Green theorem, we obtain the following equation for the filtered quantities:

$$\beta_m \frac{\partial c_m}{\partial t} + \sum_{i=1}^{N_i} \dot{\mathcal{M}}_i(t) = -\nabla \cdot \mathbf{J}_m, \tag{6}$$

where we introduced the average inter-region mass exchange rate for region i, $\dot{\mathcal{M}}_i(t)$, defined as:

$$\dot{\mathcal{M}}_i(t) = \frac{1}{V} \int_{\partial\Omega_i} \mathcal{D}'_i \frac{\partial c'_i}{\partial n} dS \tag{7}$$

and the total average flux in the mobile region, $\mathbf{J}_m$. This last quantity can be interpreted as an effective flux in the mobile region, $\mathbf{J}_{m,\text{eff}}$, defined as [44, 45]:

$$\mathbf{J}_m = \boldsymbol{u}c_m - \mathcal{D}_m \cdot \boldsymbol{\nabla}c_m \tag{8}$$

where $\boldsymbol{u}$ and $\mathcal{D}_m$ are the effective (i.e., macroscopic) velocity and the effective diffusivity (generally a tensor, hence the dot product in equation 8), which include the contribution of dispersion phenomena. Such quantities can be evaluated employing volume averaging [67] or homogenisation theory [45, 2] and in the following, we will assume they are known at each instant of time. By aplying the Favre average to the concentration in the immobile region, we obtain from eq. (1):

$$\frac{\partial c_i}{\partial t} = \frac{\dot{\mathcal{M}}_i(t)}{\beta_i}. \tag{9}$$

Finally, the multicontinuum equation for the concentration field in the mobile region can be written as:

$$\beta_m \frac{\partial c_m}{\partial t} + \sum_{i=1}^{N_i} \beta_i \frac{\partial c_i}{\partial t} = -\boldsymbol{\nabla} \cdot \mathbf{J}_m. \tag{10}$$

In the latter equation we have included the boundary conditions of the equations at the microscale (see eq. (3)) as source terms, one for each immobile region.

A key point of the MRMT formulation, is that the concentration in each immobile region is expressed as linear combination of the eigenfunctions of the diffusion operator. Therefore, the average concentration in each immobile region can be uniquely decomposed as:

$$c_i = \sum_{k=0}^{\infty} \beta_{ik} c_{ik}, \tag{11}$$

where c_{ik} is the (unknown and time dependent) coefficient corresponding to the k-th eigenfunction, and β_{ik} plays the role of a capacity relative to the k-th mode.

After performing a number of manipulations involving spectral analysis of the diffusion operator in the immobile regions [44], one can recover the classic formulation of Haggerty and Gorelick [30]:

$$\begin{cases} \beta_m \dfrac{\partial c_m}{\partial t} + \displaystyle\sum_{i=1}^{N_i} \beta_i \sum_{k=1}^{\infty} \beta_{ik} \dfrac{\partial c_{ik}}{\partial t} = -\boldsymbol{\nabla} \cdot \mathbf{J}_m \\[2ex] \dfrac{\partial c_{ik}}{\partial t} = \lambda_{ik}\left(c_{ik} - c_m\right), \quad \begin{array}{l} i = 1, \dots, N_i \\ k = 1, \dots, \infty \end{array} \end{cases} \tag{12}$$

where λ_{ik} is the eigenvalue corresponding to the k-th eigenfunction, which can be written in dimensionless form as:

$$\lambda_{ik} = \alpha_{ik}\omega_i, \tag{13}$$

where $\omega_i = \frac{\mathcal{D}'_i}{L_i}$ is specific for each immobile region, with L_i the characteristic length of the i-th immobile region. Notice that the values of α_{ik} can be computed for any geometrical configuration of the immobile region i following the approach described in Municchi and Icardi [44].

3. Numerical implementation in OPENFOAM®

3.1. Discretisation method

The governing equations 13 are discretised by means of the Finite Volume Method (FVM), which consists in integrating the governing equations over a set of control volumes (cells) on a numerical mesh. Furthermore, one assumes

that the cells are sufficiently small that all fields can be assumed to vary linearly within each cell [42]. Therefore, system (12) is written in the finite volume formulation:

$$
\begin{cases}
\displaystyle \int_{V_c} \left[\beta_m \frac{\partial c_m}{\partial t} + \sum_{i=1}^{N_i} \sum_{k=1}^{\infty} \beta_{ik} \frac{\partial c_{ik}}{\partial t} \right] \mathrm{d}V = \sum_{f=0}^{N_{c,f}} \oint_{S_{c,f}} \left(\mathcal{D}_m \cdot \boldsymbol{\nabla} c_m - \boldsymbol{u} c_m \right) \cdot \boldsymbol{n}_{c,f} \mathrm{d}S \\[4mm]
\displaystyle \int_{V_c} \left[\frac{\partial c_{ik}}{\partial t} - \lambda_{ik} \left(c_{ik} - c_m \right) \right] \mathrm{d}V = 0, \quad \begin{array}{l} i = 1, \dots, N_i \\ k = 1, \dots, \infty \\ c = 0, \dots, N_c \end{array}
\end{cases}
\tag{14}
$$

where the index c runs from 0 to the number of cells in the mesh N_c, while the index f runs from 0 to the number of faces $N_{c,f}$ belonging to cell c. Furthermore, V_c is the volume of cell c while $S_{c,f}$ and $\boldsymbol{n}_{c,f}$ are respectively the surface and surface normal of face f in cell c.

Using the assumption of linearity within each cell and using the subscripts e and f to indicate fields evaluated at the cell and face center respectively, one obtains the discretised system:

$$
\begin{cases}
\displaystyle \beta_{m,c} \frac{\partial c_{m,c}}{\partial t} + \sum_{i=1}^{N_i} \sum_{k=1}^{\infty} \beta_{ik,c} \frac{\partial c_{ik,c}}{\partial t} = \frac{1}{V_c} \sum_{f=0}^{N_{c,f}} \left(\mathcal{D}_{m,f} \cdot (\boldsymbol{\nabla} c_m)_f - \boldsymbol{u}_f c_{m,f} \right) \cdot \boldsymbol{n}_{c,f} S_{c,f} \\[4mm]
\displaystyle \frac{\partial c_{ik,c}}{\partial t} - \lambda_{ik,c} \left(c_{ik,c} - c_{m,c} \right) = 0, \quad \begin{array}{l} i = 1, \dots, N_i \\ k = 1, \dots, \infty \\ c = 0, \dots, N_c \end{array}
\end{cases}
\tag{15}
$$

where the spectral expansion is then truncated such that $k = 1 \dots M$ where M is the number of terms in the expansion to be retained.

The FVM requires the definition of appropriate discretisation operators to express face-based variables like $(\nabla c_m)_f$ and $c_{m,f}$ as cell-based variables (e.g., $c_{m,c}$). A number of such discretisation methods (e.g., Gauss integration based linear and upwind schemes) are available in OPENFOAM® [9, 25] and they will not be discussed here since their effectiveness depends on the specific problem to solve. Unlike previous works [58], the equations for the immobile regions are discretised in time and solved separately and iteratively rather than being included in the equation for the mobile region. While this leads to larger memory requirements and requires a more complex software architecture [58], it also results in a more flexible code. Most importantly, it allows to include more complicated physical models in the future and to couple the equations in an implicit manner through multiple iterations.

The *multiContinuumModels* library we are discussing here is publicly available at [49].

3.2. Library structure

The *multiContinuumModels* library [49] follows a flexible object oriented structure. This allows to easily implement new functionalities with relative ease. A base abstract class named *multiContinuumModel* store references to concentration c_m and capacity β_m in the mobile region, and provides public functions for calculating the source term $\dot{\mathcal{M}}$ as well as for updating the model describing the immobile regions. These are the only functions that need to be called inside an OPENFOAM® application to make use of this library.

The *multiContinuumModel* class is base for the *multiRateMassTransfer* class, which holds a list of pointers to *immobileRegion* objects (representing the transfer models for each immobile region) and stores the total concentration in the immobile regions $\sum_i c_i$. This class also implements the function that returns the overall source term $\dot{\mathcal{M}}$.

Classes derived from the *immobileRegion* abstract class are at the core of the multi-rate model, since they implement different kind of transfer models based on the geometrical and physical properties of the medium. Each immobile region holds a list of pointers to fields representing the concentration c_{ik} corresponding to each term in the multi-rate series. The length of such array is given by the *nOfTerms* label, and is read at the beginning of the simulation. Furthermore, this class stores the concentration in the immobile region c_i, the relative capacity β_i, and the frequency ω_i. These are all fields, and can be defined by the user as uniform or non-uniform (e.g., non-uniform initial condition on c_i, spatially varying capacity β_i and medium properties ω_i). This class also implements a function that solves the system of ODEs for the multi-rate terms. The multi-rate coefficients α_{ik} and β_{ik} are computed in derived classes, specialised for spheres, layers, cylinders, and first order regions. The user can easily develop new derived classes given for specific geometries and diffusion processes, by defining the multi-rate parameters.
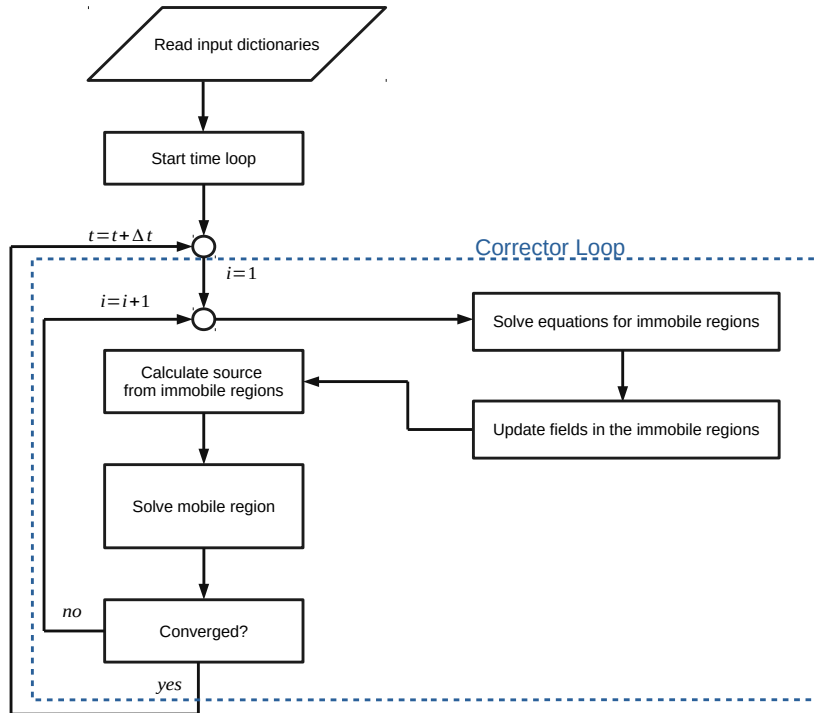
Figure 2: Diagram showing the numerical algorithm for *multiRateScalarTransportFoam*.

3.3. *multiRateScalarTransportFoam*

The library includes an application for solving the scalar transport equations with the multi-rate mass transfer model. Such application, named *multiRateScalarTransportFoam*, solves the system of equations 15, corresponding to the multi-rate model of Haggerty and Gorelick [30]. The solver is based on the standard *scalarTransportFoam* available in native OPENFOAM® and employs a special *multiContinuumControl* object (derived from the PIMPLE algorithm in OPENFOAM®) that wraps the *multiContinuumModel* library and checks for convergence.

The complete solution algorithm (including operations performed by the *multiContinuumModel* library) is illustrated in Figure 2, and it consists in a time loop with a nested corrector loop possessing a sub-time stepping loop. These operations can be summarised as follows:

- **Corrector loop**: this is the principal solution step. It consists in solving the governing equations for the immobile regions (with the optional sub-time stepping) and the advection-diffusion equation for the mobile region sequentially, in a segregated manner. When the residuals fall below a certain threshold or the maximum number of iterations (defined by the user) has been reached, the solver exits the loop.

- **Time loop**: it constitutes the main loop. After a satisfactory solution has been achieved in the corrector loop, the algorithm moves on to the next time step.

3.4. Input files

Input data and controls are provided by mean of appropriate 'dictionaries' (i.e., input files in OPENFOAM® terminology). In the *multiContinuumModel* library, input parameters must be provided in the *multiRateProperties* dictionary located in the folder *constant* (see the OPENFOAM® [50] details regarding the structure of simulation folders).

3.4.1. *multiRateProperties dictionary*

Listing 1 shows an example of basic input for the *multiRateProperties* dictionary. The first lines (1 to 8) are the required OPENFOAM® header, and are present in all dictionaries in a similar fashion. Lines 11 and 12 control the time-

step adaptivity. In fact, the library allows to automatically set the time step Δt in such way that the mass-transfer-based Courant number satisfies:

$$Co_\lambda = \max\left(\alpha_{ik}\omega\right)\Delta t < Co_{\max}, \tag{16}$$

where $Co_{\max}$ is the read from line 12. Ensuring that $Co_\lambda < 1$ is a necessary condition to obtain accurate and bounded results and therefore it is highly advised to keep this option active. However, in many applications (as groundwater transport) the time scale corresponding to the transport in the mobile region will be much smaller than the time scale of the mobile-immobile transfer. Therefore, in most circumstances the time step will not need to be adjusted.

Lines 14 to 24 of listing 1 contain the list of immobile regions. Each region is specified as a sub-dictionary with a user-defined name, which will be used by the library to identify the region and build the appropriate fields. Lines 16 to 23 show one immobile region as example. All immobile regions have the following entries:

- type: this is the type of immobile region, which defines how the α_{ik} and β_{ik} are computed.

- numberOfTermsInExpansion: defines how many terms should be retained in the expansion.

- rescaleBetas: this entry allows to decide how the truncation of the series is handled. If set to true, all β_{ik} are rescaled such that $\sum_k \beta_{ik} = 1$ as in [58]. By default, this entry is set to false and a 'truncation capacity' $\beta_{tr} = 1 - \sum_k \beta_{ik} \neq 0$ will be computed. This truncation capacity will then be added to the capacity of the mobile region, as if the truncated terms were in equilibrium with the mobile concentration [44].

```
1   FoamFile
2   {
3       version         2.0;
4       format          ascii;
5       class           dictionary;
6       location        "constant";
7       object          multiRateProperties;
8   }
9
10  //- Controls for time-step adaptivity
11  adaptiveTimeStepping        true;
12  maxCo                       0.95;
13
14  immobileRegions //- List of immobile regions
15  (
16      nameOfRegion //- This can be any name
17      {
18          //- Type of immobile region
19          type                    Spheres;
20
21          //- Terms to represent the immobile region
22          numberOfTermsInExpansion        50;
23
24          //- How the truncation is handled
25          rescaleBetas            false;
26      }
27  );
```

Listing 1: Basic input for the *multiRateProperties* dictionary

3.4.2. *Immobile regions*

At the current stage, there are four different immobile region types available: Spheres, Cylinders, Layers, and a region for which mass transfer is given by a linear first-order process. We refer to the latter a first-order region. Table 1 shows how the values of α_{ik} and β_{ik} computed for different immobile regions. Since the zeros of the Bessel function are not computed explicitly, but are stored in an array, cylindrical immobile regions are limited to 50 terms in the expansion. First-order regions are the most flexible kind of immobile region, since the values of α_{ik} and β_{ik} are read directly from the dictionary. This makes this type of immobile region appropriate for calibration studies.

Type	α_{ik}	β_{ik}
Layers	$\dfrac{(2k-1)^2 \, \pi^2}{4}$	$\dfrac{8}{(2k-1)^2 \, \pi^2}$
Cylinders	ζ_k^2	$\dfrac{4}{\zeta_k^2}$
Spheres	$k^2\pi^2$	$\dfrac{6}{k^2\pi^2}$
FirstOrderRegions	alphaCoeffs	betaCoeffs

Table 1
Expressions for α_{ik} and β_{ik} for different types of immobile regions. Here ζ_k corresponds to the k-th zero of the 0-Bessel function of the first kind. The eigenvalues λ_{ik} can be obtained using eq. (13) and the ω reported in tables 3 and 4

Listing 2 shows the syntax for a first-order region. Notice that the number of entries in alphaCoeffs and betaCoeffs must be equal to numberOfTermsInExpansion.

```
1
2       immobile
3       {
4           type                        FirstOrderRegions;
5           numberOfTermsInExpansion                    3;
6           alphaCoeffs                nonuniform (1  2  3);
7           betaCoeffs              nonuniform (0.5  0.3  0.2);
8       }
```

Listing 2: Example of a FirstOrderRegions immobile region (named 'immobile') with three terms

In addition to being defined in *multiRateProperties*, immobile regions require a set of fields representing the initial condition, the capacity, and the transfer rate. These fields can be summarised (for each immobile region) as:

- c.<name of region>: is the field representing the field c (Favre averaged concentration) in that immobile region. It is possible to specify an initial condition for this field following the standard OPENFOAM® syntax [50].

- omega.<name of region>: is the field representing the transfer rate for that immobile region. This field represents the material properties related to a immobile region and can vary in space and time. Specifically, it coincides with the ration between the diffusion coefficient and the square of a reference length for all region types except FirstOrderRegions.

- beta.<name of the region>: represents the capacity of the immobile region, and can vary in space and time.

The *tutorials* folder in the library [49] provides a range of examples illustrating the syntax and how to structure a simulation folder.

4. Results and discussion

In this Section we show applications of our library in different situations taken from problem settings in heterogeneous porous media and flow in packed bed equipment. We choose the different systems mainly to show the the flexibility of our model and implementation in different situations, but they also have the purpose to show the wide range of applicability of such a model. We start from a simple $0D$ model and then we move to more realistic-like cases in following sections.

One important numerical parameter investigated is M, the number of terms of expansions terms, (i.e. we truncate the infinite series of eigenfunctions in eq. (15) after M terms). The truncation is handled differently depending on the flag `rescaleBetas`, as described in section 3.4.1. In table 2 we summarise all the cases we consider in the following specifying the different geometries considered along with their relevant initial and boundary conditions. These are

	0D		
	$c_m(t=0)$	$c_{im}(t=0)$	$c_{m,inlet}$
7SP	1	0	-
	1D		
	$c_m(t=0)$	$c_{im}(t=0)$	$c_{m,inlet}$
First-order	0	1	0
1SP	1	0	0
	2D		
	$c_m(t=0)$	$c_{im}(t=0)$	$c_{m,inlet}$
7SP	1	0	0
COMP	1	0	0
RAND2D	1	0	0
	3D		
	$c_m(t=0)$	$c_{im}(t=0)$	$c_{m,inlet}$
7SP	1	0	0

Table 2
Summary of the setup of the cases considered here. $c_m(t=0)$ and $c_{im}(t=0)$ are the initial concentrations of the mobile and immobile regions respectively, inside the domain. $c_{m,inlet}$ is the boundary condition at the inlet for the mobile concentration.

	ω_i (s^{-1})	β_i
Sphere1	$3.1 \cdot 10^{-8}$	0.0406
Sphere2	$9.2 \cdot 10^{-8}$	0.1699
Sphere3	$2.3 \cdot 10^{-7}$	0.2731
Sphere4	$2.7 \cdot 10^{-7}$	0.2592
Sphere5	$9.4 \cdot 10^{-7}$	0.1548
Sphere6	$1.7 \cdot 10^{-6}$	0.0620
Sphere7	$1.4 \cdot 10^{-6}$	0.0404

Table 3
Values of ω_i (where $i = 1, \ldots, 7$) and capacity coefficients β_i as reported in Tab.2 of Haggerty and Gorelick [30] used for the calculation of the 7SP model.

particularly important as they define the kind of mass-transfer happening in the system and the effect of the immobile regions. Most cases are solved for empty immobile regions and fully saturated mobile regions, resulting in a maximum transfer in the initial transient. In presence of an inflow with concentration zero (1D, 2D, 3D), the initial mass in the system is all flushed away with the immobile regions slowing down the process, storing temporarily some mass. The stationary state in this case, is when the system is completely empty with all concentrations equal to zero. All the cases we present in this section are included in the library package as tutorials.

4.1. Zero-dimensional test-case

For the zero-dimensional test-case, we solve eq. (14) in OPENFOAM®in a domain composed by a single cell. In this way, we obtain a configuration akin to that described in Haggerty and Gorelick [30] for batch reactors (no advection, dispersion, sources and sinks). We choose to represent the immobile region as composed by seven spherical immobile regions, and we called this the 7SP model. This is analogous to the one reported in Tab.2 of Haggerty and Gorelick [30], with the same β and ω which we report in table 3. Our purpose here is to compare our results with those of Haggerty and Gorelick [30] to demonstrate the accuracy of our implementation.

We report the results for four different numbers of retained eigenfunctions in the expansion, identified by $M = 2, 10, 20, 50$, in terms of the normalised concentration of the mobile region $\hat{c}_m$, defined as

$$\hat{c}_m = \frac{c_{eq} - c_m(t)}{c_{eq} - c_m(t=0)}, \tag{17}$$

where c_{eq} is the equilibrium concentration between mobile and immobile regions, $c_m(t=0)$ is the initial concentration
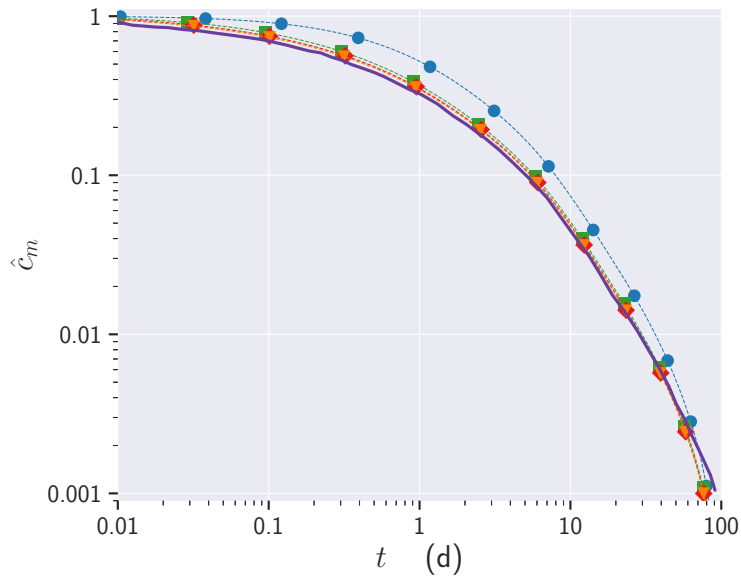
Figure 3: Breakthrough curves at different expansion for the 7SP model (see table 3) compared with the same model reported in Haggerty and Gorelick [30]. The purple continuous line is taken from [30] (Table 2), blue • $M=2$, green ■ $M = 10$, red ◆ $M = 20$, orange ▼ $M = 50$

in the mobile regions, $c_m(t)$ concentration in the mobile region at time t. The curve we obtain is shown in fig. 3. As it can be seen, using only two terms (i.e. $M = 2$) is not sufficient to capture the dynamics of the process. However, $M = 10$ seems already enough to obtain good quantitative agreement with the known results (see Figure 2-b in [30]). As expected, the agreement increases as we increase the number of expansions. However, notice that our method is prescribing a slightly different trend due to the way we account for the truncated terms (without rescaling), which is not detailed in [30].

4.2. One-dimensional test cases

In the following, we discuss two one-dimensional test cases characterised by one single first-order and sphere regions.

4.2.1. First-order immobile regions

In order to assess the accuracy of our numerical method and the correct implementation of the library, we compare results from the `multiRateScalarTransportFoam` numerical solver described in section 3.3 against a spectral solution for a simple problem with advection and diffusion. We therefore consider the following system of equations:

$$\begin{cases} \dfrac{\partial c_m}{\partial t} + \dfrac{\partial c_m}{\partial x} - \dfrac{1}{10} \dfrac{\partial^2 c_m}{\partial x^2} = \dfrac{1}{2} \left(c_i - c_m \right) \\ \dfrac{\partial c_i}{\partial t} = \left(c_m - c_i \right) , \end{cases} \tag{18}$$

together with the following boundary conditions:

$$\left. \dfrac{\partial c_i}{\partial x} \right|_{x=0} = \left. \dfrac{\partial c_i}{\partial x} \right|_{x=1} = 0, \quad c_m(t,0) = 0, \quad \left. \dfrac{\partial c_m}{\partial x} \right|_{x=1} = 0, \tag{19}$$

and initial conditions:

$$c_m(x, t=0) = 0, \quad c_i(x, t=0) = 1. \tag{20}$$

Notice that the coefficients appearing in system 18 are chosen arbitrarily to generate fast transients dominated by convection and mass transfer, and do not necessarily represent any realistic application to groundwater flows. However, they provide an excellent test for the numerical stability of this algorithm and the relatively large diffusion allows for efficient spectral solutions.

In this simplified mathematical model, at time $t = 0$ mobile and immobile regions begin exchanging mass, starting from a condition of non-equilibrium. Specifically, mass is transferred from the immobile region to the mobile region and then transported out of the domain by advection. System 18 is solved using the Matlab-based library CHEBFUN [24], which employs Chebyshev polynomials to solve systems of differential equations to spectral accuracy, providing our benchmark solution. System 18 is discretised in OpenFOAM®using a second order schemes in space (i.e., `linearUpwind` scheme for advection and `Gauss linear`, i.e., central differences, for diffusion) and in time (`backward` scheme). A grid of 20 cells was used and the time step was chosen dynamically to satisfy the Courant-Friedrichs-Lewys condition $Co = U \Delta t / \Delta x < 1$ [15], where Co is the Courant number, $U = 1$, Δt is the time step, and Δx is the mesh spacing. Such time step was small enough to satisfy also the condition for Co_λ.

In the following, the quantity of interest is the normalised flux of concentration across the downstream boundary of the domain, also called the breakthrough curve:

$$BT(t) = \dfrac{\displaystyle\oint_{S_{\text{out}}} c_m(\boldsymbol{x}, t) \boldsymbol{u} \cdot \mathrm{d}\boldsymbol{S}}{\displaystyle\oint_{S_{\text{out}}} \boldsymbol{u} \cdot \mathrm{d}\boldsymbol{S}}, \tag{21}$$

where S_{out} is the outlet boundary of the domain. Furthermore, we will often look at the average concentration in the immobile regions within the domain defined as:

$$c_{im}(t) = \dfrac{\displaystyle\int_{\Omega} c_i(\boldsymbol{x}, t) \, \mathrm{d}V}{\displaystyle\int_{\Omega} \mathrm{d}V}. \tag{22}$$

Notice that c_{im} can be computed for different immobile regions. However, we will not assign a subscript i to c_{im}. Instead, we will specify in each plot which is the immobile regions we are considering.
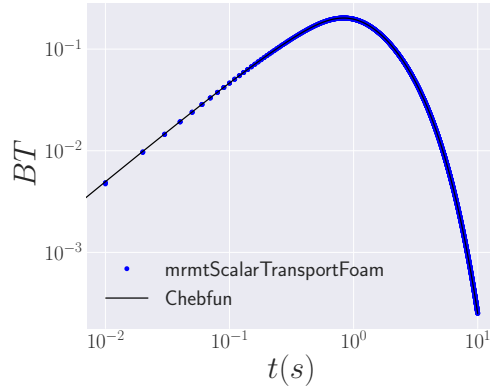
Figure 4: Breakthrough curves from CHEBFUN [24] and our OPENFOAM® solver `multiRateScalarTransportFoam`. The root mean square deviation between the two methods is 0.33%.

As it can be seen in Figure 4, there is an excellent agreement between the breakthrough curve predicted by CHEB-FUN and that predicted by `multiRateScalarTransportFoam`. In the initial times, there is a sharp increase in the breakthrough curve cause by concentration being mobilised and flushed out. After reaching a peak, the diffusion out of the immobile region and subsequent advection-diffusion out of the domain decays exponentially to zero. This is expected as we used a single-rate mass transfer model.

4.2.2. Spherical immobile regions

In this testcase, we solve again system 18, replacing the RHS single-rate mass transfer with the multi-rate expansion of a single sphere. Therefore we denote it by 1SP. Contrarily to the previous case, the immobile regions start here completely empty, and all the concentration is initially in the mobile part of the system.

Results are presented in figure 5 for various numbers of terms in the eigenfunction expansions, and different values of *omega* and *beta* for the spherical inclusions. Other simulations parameters are identical to those in 4.2.1.

Figure 5a shows the results for $\omega = 1.0$ and $\beta = 0.1$, which represent the maximum value of ω and the minimum value of β we probed. Such values result in very large eigenvalues corresponding to characteristic response times $\tau_k = \alpha_k \omega^{-1} > 1$, which leads to a very fast mass transfer that is dominated by leading order term in the expansion. Furthermore, the low value of β (compared to the size of the mobile region) means that the spheres have low capacity. Therefore, it is expected that a small number of terms in the expansion would be enough to capture the system dynamics, which consists in a fast evolution with little or negligible non-local effects. This is precisely what is observed in figure 5a (where increasing the number of terms does not result in any significant change and are therefore omitted).

Conversely, decreasing ω leads to slower transients due to the slower response time of the modes. Therefore, the role of time history on the system dynamics increases from figure 5b to 5d, and a larger number of terms is required to capture the fast transients. In fact, the leading order term corresponds to the slowest dynamics (the smallest eigenvalue) and it is often the only one retained in asymptotic theories (where the initial transient is disregarded). It is however necessary to retain a large number of terms in order to accurately predict non-equilibrium dynamics. It should be noted that the capacity is also playing an important role. When the capacity of the system increases and approaches the limit of infinite capacity (i.e., infinite size) of the immobile regions the slope of the breakthrough approaches $-3/2$ [37] as shown in figure 5d.
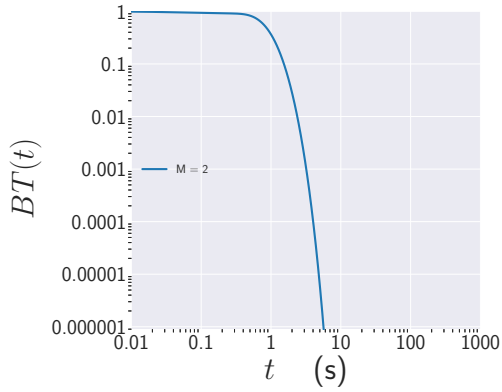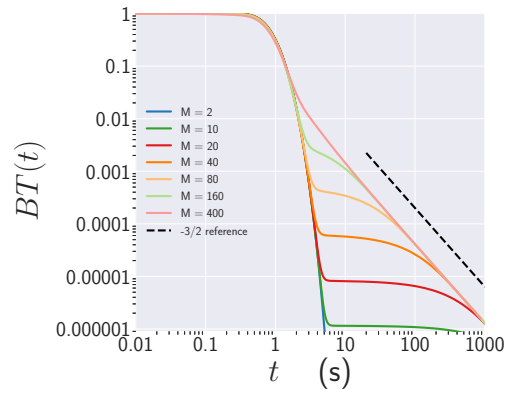
(a) $\omega = 1.0 \text{ s}^{-1}$, $\beta = 0.1\,\beta_m$
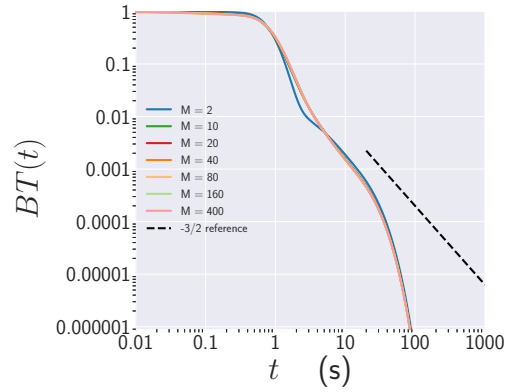
(b) $\omega = 0.01 \text{ s}^{-1}$, $\beta = 1\beta_m$
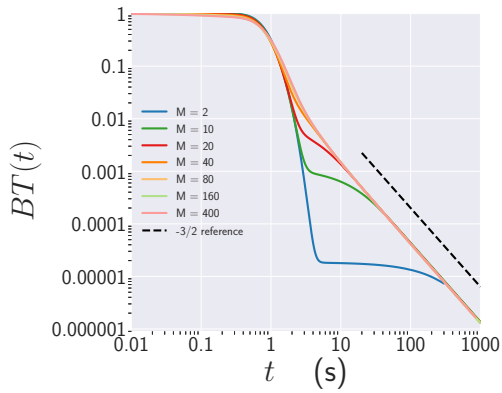
(c) $\omega = 10^{-4} \text{ s}^{-1}$, $\beta = 10\,\beta_m$

(d) $\omega = 10^{-6} \text{ s}^{-1}$, $\beta = 100\,\beta_m$

Figure 5: Breakthrough curves for the 1Sp model at different values of ω and β for different expansion numbers. The top-left plot reports just a single curve since they are all coincident

4.3. Two-dimensional simulation of heterogeneous porous media

In this section, we apply `multiRateScalarTransportFoam` to solve for solute transport in media characterised by spatially variable properties. The modelling of transport of dissolved substances and energy in heterogeneous porous media is a key issue in a series of applications ranging from groundwater remediation [22] to radionuclide migration [55], and the geological storage of carbon dioxide [53].

The computational domain considered here is a 2D domain of width 2 m and height 1 m. The numerical grid was built in OPENFOAM®using the `blockmesh` utility, which allows the generation of orthogonal hexahedral meshes. The total number of cell in our computational domain is 20000.

4.3.1. Flow and permeability fields

In all the subsequent cases, the flow field in the porous media is obtained by solving the steady-state Darcy equation:

$$-\mu^{-1}\mathbf{K} \cdot \nabla P = \mathbf{u}\,, \quad \nabla \cdot \mathbf{u} = 0\,, \tag{23}$$

where μ is the dynamic viscosity of the fluid, K is the permeability tensor, and P is the pressure. In this work we considered the dynamic viscosity of water at 298 K, $\mu = 8.9 \cdot 10^{-4}$ Pa s. Equation 23 is solved with boundary conditions on the pressure imposing a pressure drop ΔP between the two ends of the computational domain. From eq. (23) we obtain a Poisson equation whose solution is easily implemented in OPENFOAM®. The velocity is the computed from the fluxes of the Poisson equation. This last passage is the finite volume equivalent of calculating $\mathbf{u}$ using equation 23 (with the solenoidal velocity condition). In general, the permeability field $\mathbf{K}$ is an anisotropic tensorial field which can be constant in the domain, or spatially variable. We consider here an isotropic permeability field of the form $\mathbf{K} = k(\mathbf{x})\mathbf{I}$, with $\mathbf{I}$ being the identity tensor and $k(\mathbf{x})$ a Gaussian random field. A key feature of natural and engineered porous media is, in fact, spatial heterogeneity. We model the spatially varying permeability as a realisation of a Log-Normal spatial random field, with $\log(k)$ a Gaussian random field with zero mean and unit variance. We assume an exponential correlation between the points with correlation length equal to 0.5 and 0.1, in the longitudinal and vertical direction respectively. The resulting random field is shown in figure 6a.

We solve eq. (23) with a pressure drop of $\Delta P = 10^{-6}$ Pa (which translates to Dirichlet boundary conditions of $P(0, z) = 10^{-6}$ Pa and $P(L, z) = 0$ Pa). The resulting flow-field for the permeability field shown in 6a in reported in fig. 6b. As expected, the higher velocities corresponds to regions with higher permeability K.

In the following we consider solute transport in theses spatially variable flow fields combined with mobile-immobile mass transfer characterised by constant and spatially variable properties. From a phenomenological point of view, mobile-immobile mass transfer can be considered to account for the impact of small-scale medium heterogeneities, while large scale variability is accounted for explicitly [14].

For the case of constant MRMT parameters, we will analyse two different models: *i*) the 7SP model that we discussed in section 4.1 (see also table 3), *ii*) the *Composite* (COMP) model summarised in table 4 that is a combination of different immobile regions. For the case of heterogeneous MRMT parameters, the *Random* (RAND2D) model consists in one immobile spherical region for which all the relevant parameters K, β_i, and ω_i are non-uniform and dependent on k.

4.3.2. Homogeneous mass transfer properties

We will mainly focus our discussion on the 7SP model and at the end of the section we will show some results for the COMP model.

7SP Model:

Results for the 7SP model ares reported in fig. 7a. Here, we only show the curve for $M = 2$ expansion terms. For larger M the results change only slightly on the scale of the plot. The immobile regions are initially empty (i.e. $c_{im} = 0$) and the mobile region is uniformly initialised with value $c_m > 0$.

Notice the change in the slope at the very beginning of the curve, which is reported in more detail in the inset in fig. 7a for all the different expansion. This variation in due to the fact that we started from a non-equilibrium situation, where the immobile regions are completely empty and the beginning of the simulation is dominated by the exchange between mobile and immobile regions. Notice that using a different number of modes leads to different results up to $M > 10$, after which the breakthrough curve does not change significantly and the dynamic described is much faster that the one obtained with two modes only. That is because, in this case, two modes are insufficient to capture all the relevant characteristic times of the system. Conversely, ten modes are enough to capture all the relevant time scales
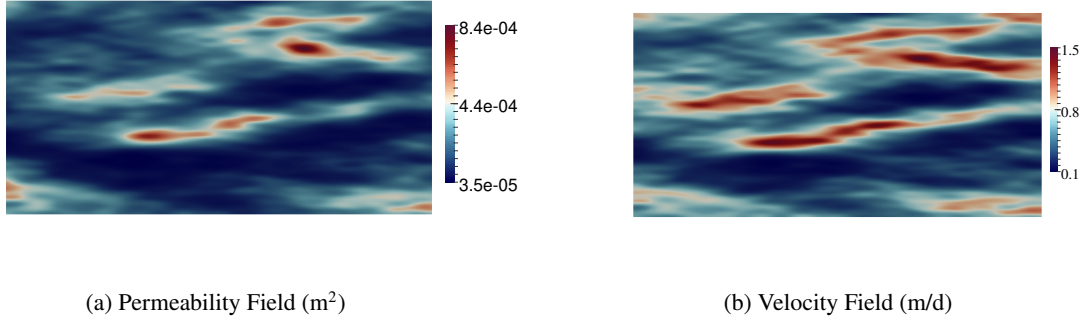
(a) Permeability Field (m²)

(b) Velocity Field (m/d)

Figure 6: Contour plot of the randomly generated permeability field and the corresponding velocity field obtained by solving eq. (23)

	ω_i (s^{-1})	β_i
Sphere1	$2.80 \cdot 10^{-7}$	0.35
Sphere2	$1.75 \cdot 10^{-8}$	0.20
Layer1	$1.43 \cdot 10^{-9}$	0.15
Cylinder1	$1.00 \cdot 10^{-9}$	0.15
FirstOrder1	$2.76 \cdot 10^{-6}$	0.05
FirstOrder2	$4.42 \cdot 10^{-5}$	0.10

Table 4
Values of ω_i (where $i = 1, \ldots, 7$) and capacity coefficients β_i as reported in Tab.3 of Haggerty and Gorelick [30] used for the calculation of the COMP model.

of this system. Notice that the black line representing zero modes (i.e., no MRMT) starts decaying at later times with respect to the case where the MRMT model is employed. This can be explained as a consequence of choosing initial conditions $c_{im} = 0 \neq c_m$, which result in a net mass exchange from the mobile region to the immobile regions. As can be seen in fig. 7a, such mass is then released slowly at later times (a characteristic of the MRMT) at a much slower rate, since the difference in concentration between mobile and immobile regions, and consequently the net flux, is much smaller than at early times.

The rapid exchange of concentration between the mobile and immobile regions is qualitatively shown in figs. 8 and 9 where the contour plots at different times of the variation of the mobile components (fig. 8) and and immobile one (fig. 9) in the 2D domain are reported. As can be observed, the process is nearly completed after approximately one day. A more quantitative result of the time variation of the concentration into the immobile region is reported in fig. 7b, where the process of accumulation of the concentration following by its discharge can be observed for three different immobile regions.

COMP Model: The COMP model gives results similar to the one presented for the 7SP model, and they are summarised in fig. 10. We can still observe a transient at the beginning of the simulation, which however, results much faster than the one shown in the 7SP model (see fig. 7a).
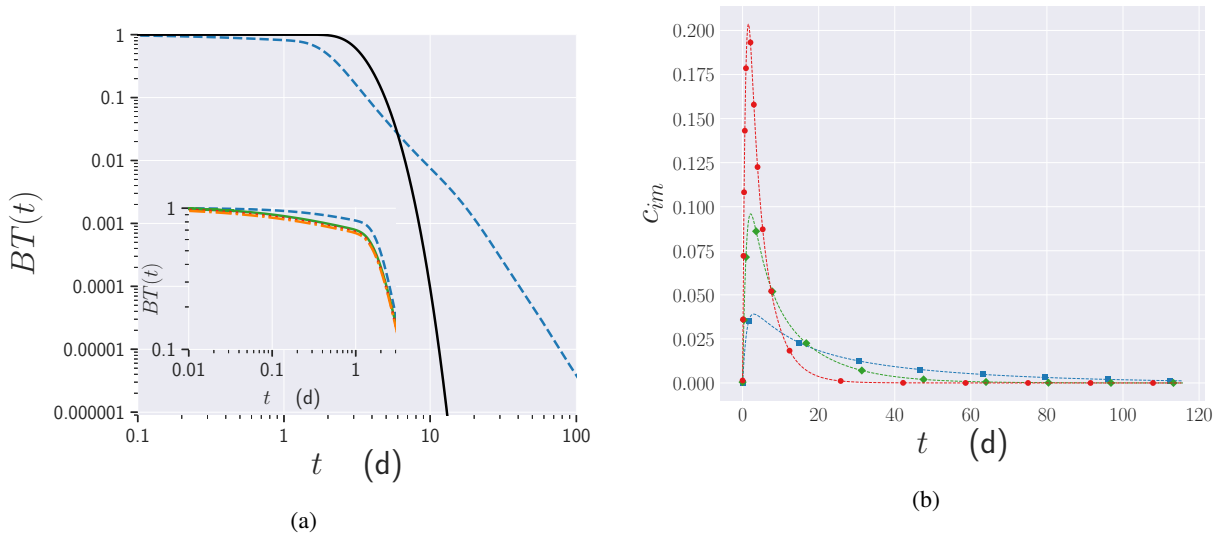
(a)

(b)

Figure 7: On the left: breakthrough curves for the 7Sp case and $M = 2$ and comparison with the case without multi-rate (black continuous curve). In the inset, are reported the results for the first 3 days for all the expansion considered: $M = 2$ dashed blue curve, $M = 10$ green continuous curve, $M = 20$ dotted curve, $M = 50$ dash-dotted curve. On the right: concentration of the concentration versus time in three of the immobile regions in the Sp7 model. Sphere2: red • $M = 10$, Sphere3: green ■, Sphere5 blue ◆.
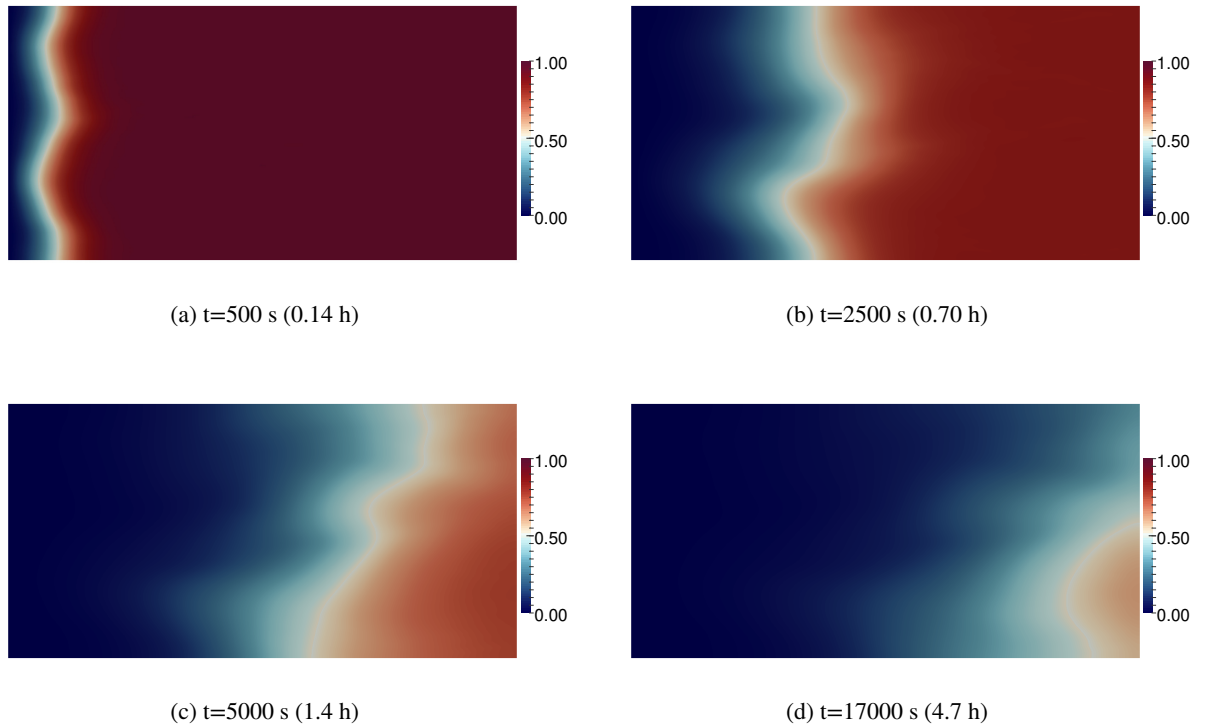

(a) t=500 s (0.14 h)

(b) t=2500 s (0.70 h)

(c) t=5000 s (1.4 h)

(d) t=17000 s (4.7 h)

Figure 8: Contour plot of the concentration of the concentration in the mobile region (kg/m³). Results are in seconds (s) and hours (h) for the sake of readability.
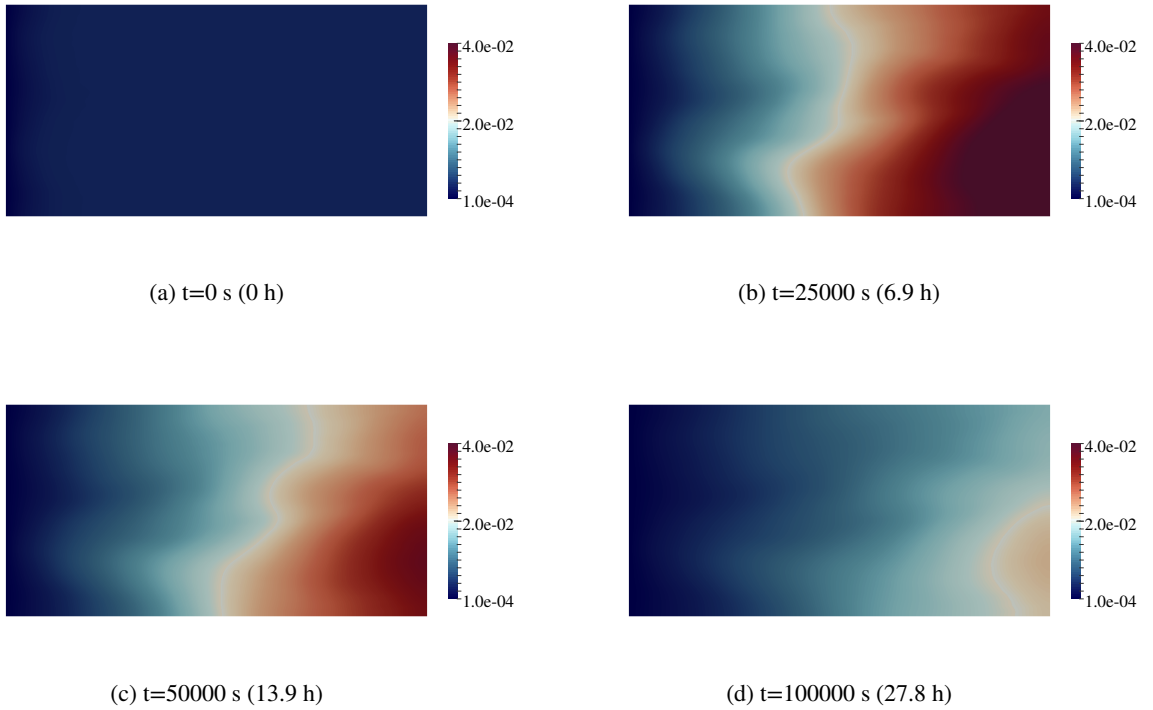
(a) t=0 s (0 h)

(b) t=25000 s (6.9 h)

(c) t=50000 s (13.9 h)

(d) t=100000 s (27.8 h)

Figure 9: Contour plot of the concentration in (kg/m³) of the concentration in the immobile region (sphere1 as defined in table 3) for the Sphere1 (see table 3). Results are in seconds (s) and hours (h) for the sake of readability.
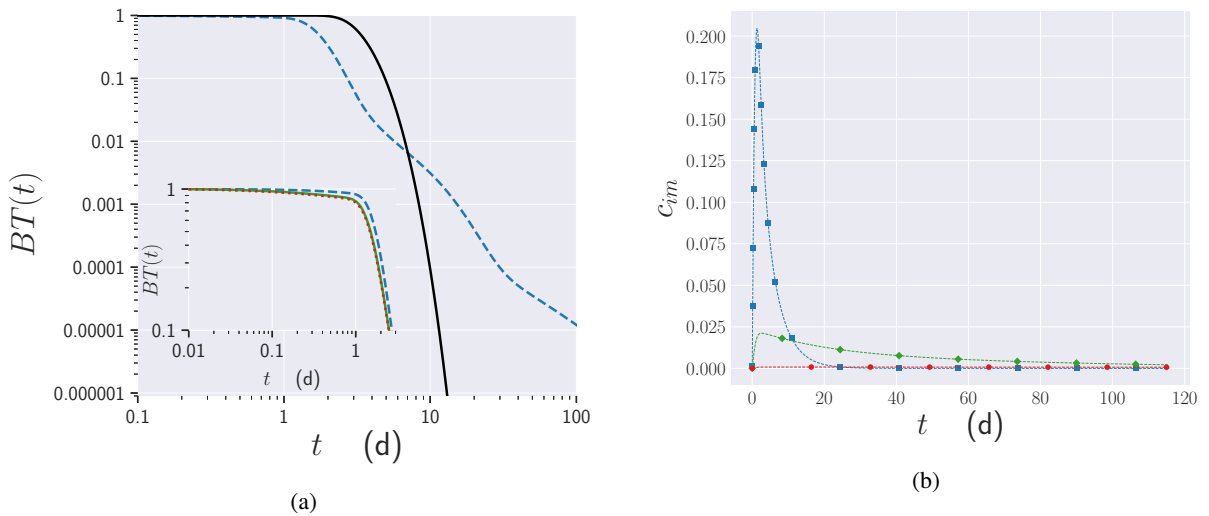

(a)

(b)

Figure 10: On the left: Breakthrough curves for the COMP case and $M = 2$ and comparison with the case without multi-rate (black dashed curve). In the inset, are reported the results for the first 3 days for all the expansion considered: $M = 2$ dashed blue curve, $M = 10$ green continuous curve, $M = 20$ dotted curve, $M = 50$ dash-dotted curve. On the right: Concentration of the concentration cm (in kg/m³) versus time in three of the immobile region in the COMP model. Sphere2: red • $M = 10$, Cylinder1: green ■, FirstOrder1 blue ◆
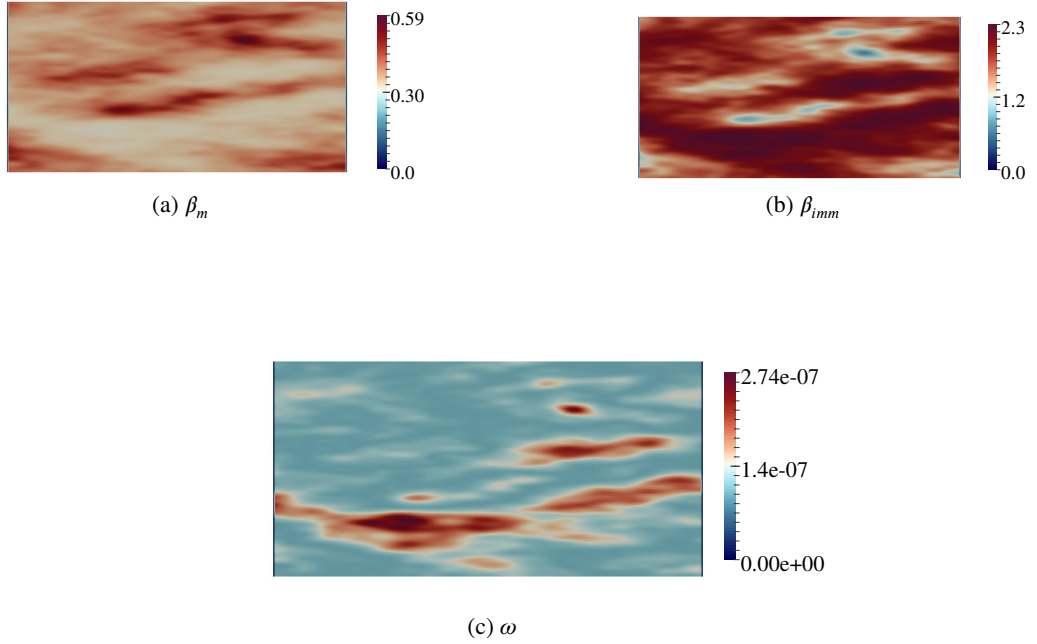
(a) β_m

(b) β_{imm}

(c) ω

Figure 11: Contour plot of the fields for β, β_{imm} and ω generated using eq. (24)

4.3.3. Heterogeneous mass transfer properties

The last case we consider for multi-rate processes in geological media is the one in which all the relevant parameters (K, α and β) are spatially distributed. Here, we consider only one immobile region modelled as a sphere.

We start by building the β_m field which we choose to be determined by K. To this end, we map the permeability random field K shown in fig. 6a into a field for β_m by associating to each k a value in [0.3, 0.6]. The final field for β_m is shown in fig. 11a. Then, we obtain for β_{im} from β_m and ω using the Kozeny-Carman law. In the end, we employ the following expressions:

$$\beta_m = 0.3 + 0.6 \frac{k - k_{min}}{k_{max} - k_{min}}, \tag{24}$$

$$\omega = a \frac{\beta_m^3}{k(1 - \beta_m)^2},$$

$$\beta_{im} = \frac{1 - \beta_m}{\beta_m},$$

where $a = 10^{-10}$, while k_{max} and k_{max} are respectively the maximum and minimum of k in the domain. These fields are shown in fig. 11.

Results, in terms of the concentration leaving the domain, and the time evolution of the concentration field in the immobile region are reported in fig. 12.

At early times, we can observe a transient similar to that observed in the previous cases (see figs. 7a and 10). In this case we notice that the peak for the average concentration in the immobile region is less pronounced than in the previous cases. However, it is interesting to notice that the breakthrough (which refers to the concentration in the mobile region) decreases faster than in the cases with homogeneous distribution.
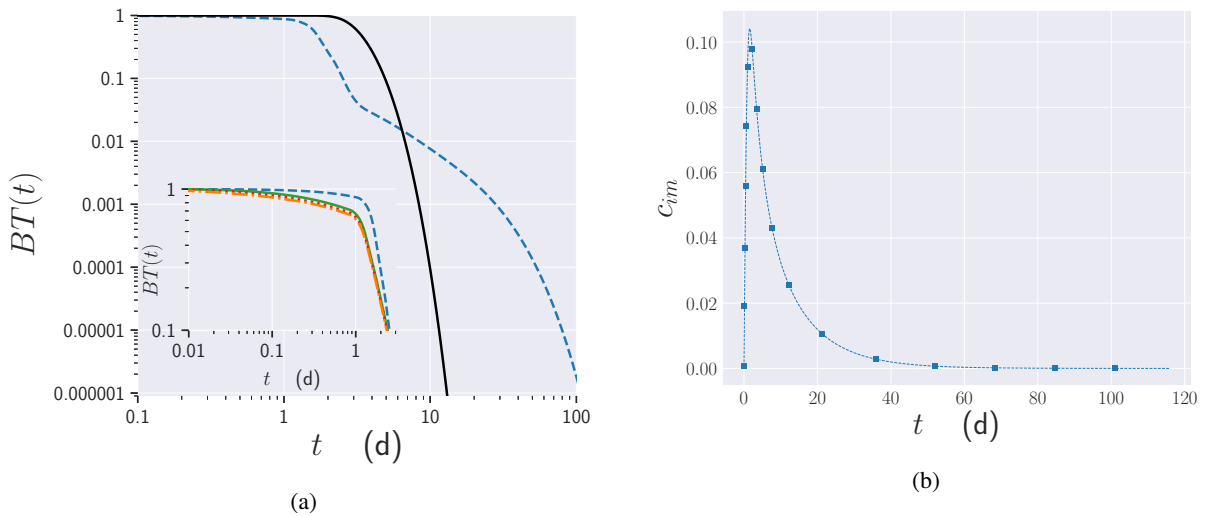
(a)

(b)

Figure 12: On the left: Breakthrough curves for the R1SP case and $M = 2$ and comparison with the case without multi-rate (black continuous curve). In the inset, are reported the results for the first 3 days for all the expansion considered: $M = 2$ dashed blue curve, $M = 10$ green continuous curve, $M = 20$ dotted curve, $M = 50$ dash-dotted curve. On the right: Concentration of the concentration c_{im} (in kg/m^3) versus time in the immobile region

4.4. Three-dimensional packed bed

The MRMT model in its current form does not include any chemical reaction terms. While the application to chemical engineering problems requires the modelling of chemical reactions, we are presenting here a proof of concept of the application of MRTM to a chemical engineering relevant problem, namely a packed bed column. The model is general enough to be used for these kinds of problems and working in our group in undergoing to include chemical reaction terms in the MRTM formulation.

Packed bed columns occupy a predominant role in chemical industry [35], where they are used in several different processes such as separation, filtration, purification or as a reaction unit and their modelling at different level and scales [29, 10, 34] which can also include the modelling of the reactions inside the domains [11]. The flow field and transport phenomena (like heat and mass transfer) inside these equipment can be described at different level of resolution, from particle-resolved models, where the components of the packing material (such as spheres) are fully described [8, 48, 47, 59], to continuum heterogeneous multiphase models [46, 13] and pseudo-homogeneous models which consider a single phase as the MRMT. Generally, bridging between different scales is not a trivial task [56].

Within the MRMT framework, the description of a packed bed with immobile particles is, on a first approximation, identical to that presented in the previous section (see section 4.3) for geological media. A steady-state Darcy equation eq. (23) can be solved on a randomly generated permeability field, while non-local transport can be modelled using the MRMT.

A three-dimensional cylindrical with height 0.5 m and base diameter of 0.06 m constituting the physical domain is discretised on a mesh composed by 64000 cells. In order to achieve an accurate and bounded solution, we employed the following discretisation schemes (we direct the reader to the OPENFOAM user guide [50] for a detailed description of each scheme):

- divergence: bounded Gauss vanLeer01 [64];

- gradient: cellLimited leastSquares 1;

- surface normal gradient: default limited 1;

These numerical schemes used ensure that the concentration of the chemical species inside the packed bed remains bounded between zero and the initial value.

Permeability and the flow field inside the domain were generated as described in the previous section by solving the steady-state Darcy equation (see eq. (23)). We used the 7Sp model described earlier (see table 3) to represent the immobile regions.

In fig. 13 we show the variation of the chemical species inside the column in the mobile region at different times. Notice that, as detailed in fig. 14, there exist two different phenomena that govern mass transport inside the packed bed: (i) mass transfer between heterogeneously distributed mobile and immobile regions and, (ii) channelling due to the heterogeneous permeability field. While the second phenomenon is most prominent in the early times, the first is responsible for the long (almost horizontal) tail in fig. 14
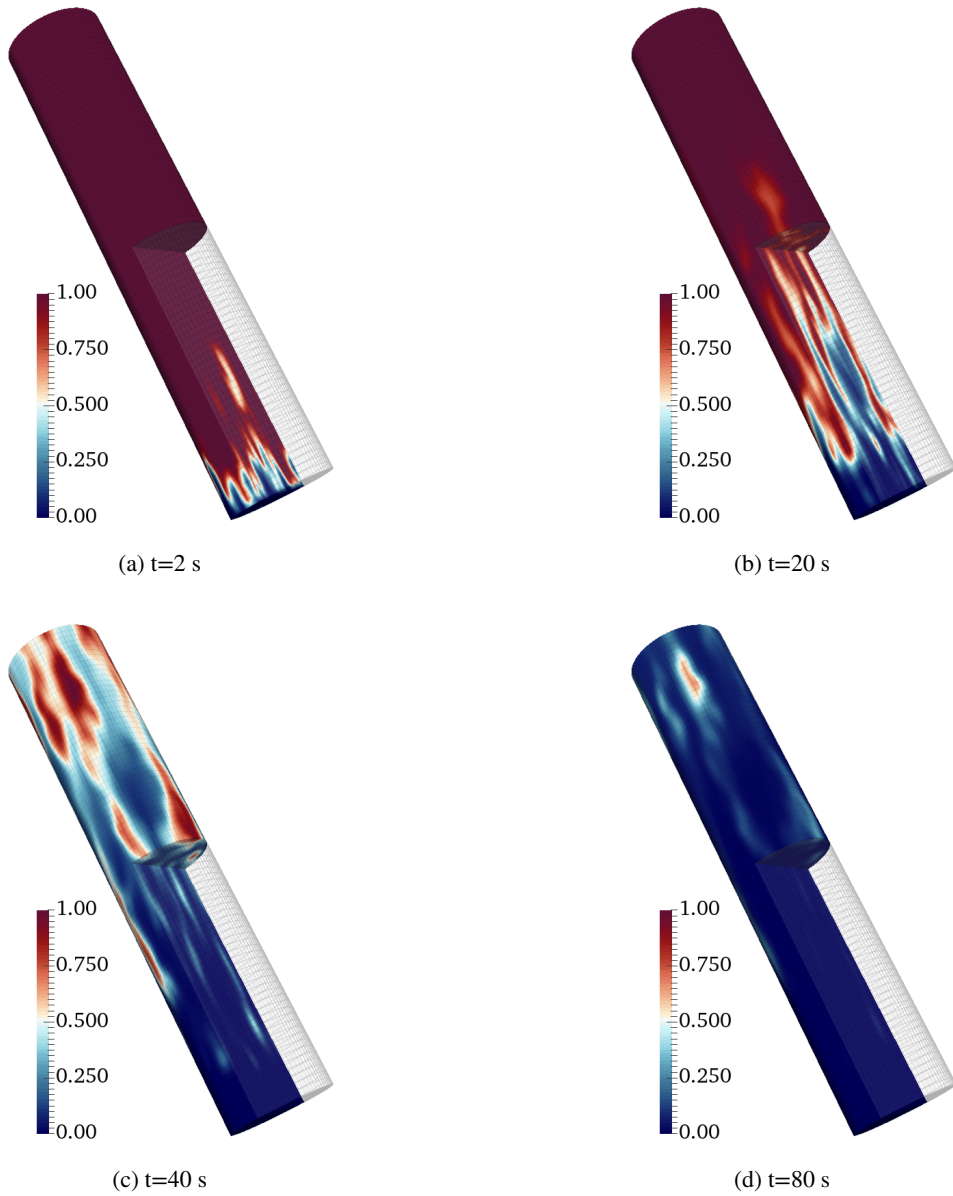
(a) t=2 s

(b) t=20 s

(c) t=40 s

(d) t=80 s

Figure 13: Contour plot of the concentration of the chemical species in (kg/m^3) in the mobile region for the Packed Bed column at different times
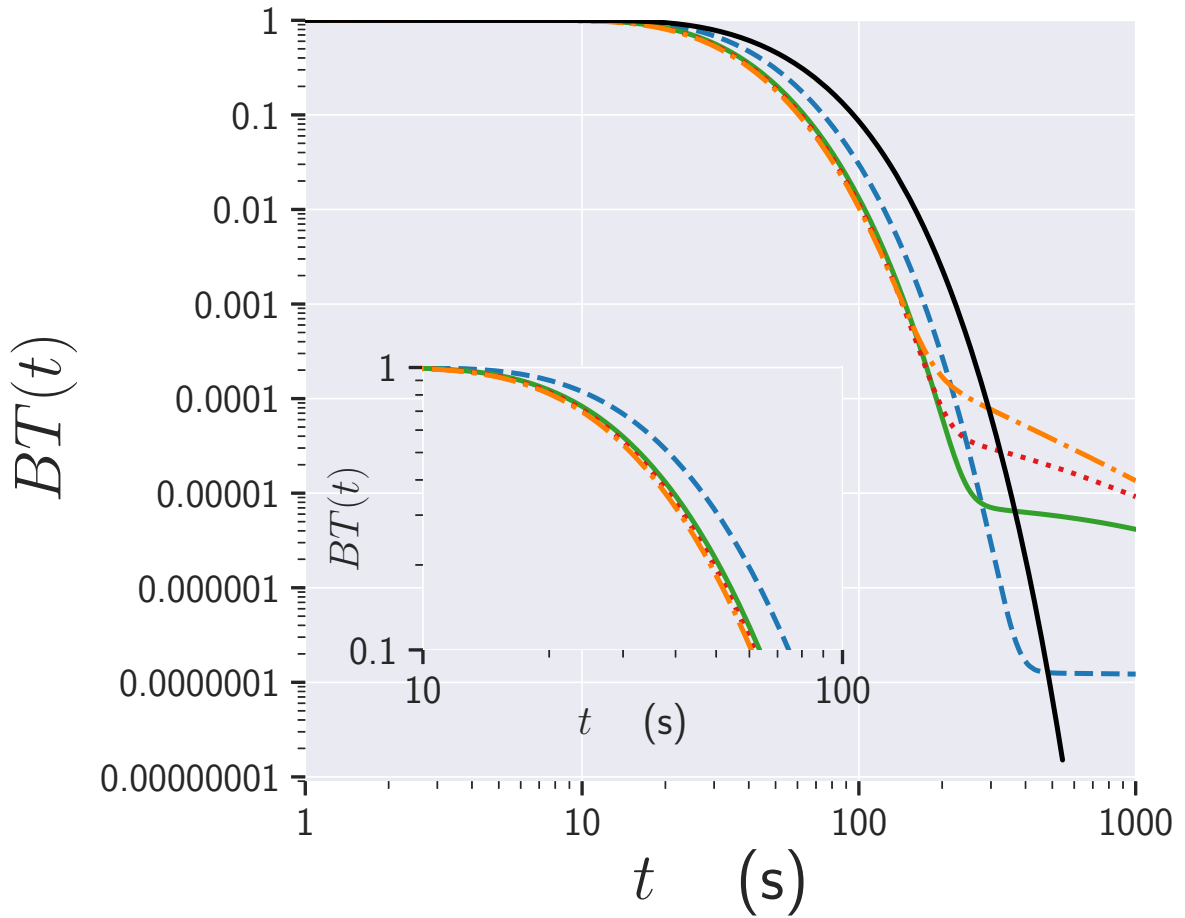
Figure 14: Breakthrough curves for the 7SP case and $M = 2$ (blue dashed curve) and comparison with the the system without multi-rate (black solid curve). In the inset, are reported the results for the first 100 seconds for all the expansion considered: $M = 2$ dashed blue curve, $M = 10$ green continuous curve, $M = 20$ red dotted curve, $M = 50$ orange dash-dotted curve.

5. Conclusions

In this work, we presented a software package included in OPENFOAM® to solve problems involving non-local (in time) transport phenomena using the Multi-Rate Mass Transfer model first proposed in Haggerty and Gorelick [30] and subsequently formalised in Municchi and Icardi [44]. Such package has been developed using the OPENFOAM® library, which has a wide range of users in academia and industry alike. The main novelties and advantages introduced in this implementation include:

- Possibility to work with heterogeneous fields such as permeability, porosity, or properties of the immobile regions within the domain.

- The OPENFOAM® technology on which this work is based allows to perform three-dimensional simulations in parallel architectures using state-of-the-art linear solvers.

- Being structured as an object-oriented C++ library, this software can be easily extended and integrated in other OPENFOAM® solvers to perform multi-physics simulations.

We showed that the the numerical solver included in the library produces results in agreement with previous works and calculations performed with CHEBFUN [24], and can reproduce results presented in literature for porous media [30, 36]. Furthermore, we proposed a number of cases that illustrate possible applications to chemical engineering and geological media, where the method is able to capture salient features of heat/mass transport. Further applications could extend to ionic transport in batteries and porous media with adsorption/desorption reactions or flow in fractures with stagnation zones.

Acknowledgements

References

[1] Adeyemo, A., Kumar, R., Linga, P., Ripmeester, J., Englezos, P., 2010. Capture of carbon dioxide from flue or fuel gas mixtures by clathrate crystallization in a silica gel column. International Journal of Greenhouse Gas Control 4, 478–485.

[2] Auriault, J., Adler, P., 1995. Taylor dispersion in porous media: Analysis by multiple scale expansions. Advances in Water Resources 18, 217–226. URL: https://ac.els-cdn.com/0309170895000117/1-s2.0-0309170895000117-main.pdf?_tid=4d9bd52b-b646-45d6-9015-6ce236801109&acdnat=1550834940_2fadb6b4d83385275f1003416e39adfehttp://linkinghub.elsevier.com/retrieve/pii/0309170895000117, doi:10.1016/0309-1708(95)00011-7.

[3] Benson, D.A., Meerschaert, M.M., 2009. A simple and efficient random walk solution of multi-rate mobile/immobile mass transport equations. Advances in Water Resources 32, 532–539.

[4] Berkowitz, B., Cortis, A., Dentz, M., Scher, H., 2006. Modeling non-Fickian transport in geological formations as a continuous time random walk. Reviews of Geophysics 44.

[5] Berkowitz, B., Emmanuel, S., Scher, H., 2008. Non-Fickian transport and multiple-rate mass transfer in porous media. Water Resources Research 44.

[6] Berkowitz, B., Scher, H., 1998. Theory of anomalous chemical transport in random fracture networks. Physical Review E 57, 5858.

[7] Berkowitz, B., Scher, H., 2009. Exploring the nature of non-fickian transport in laboratory experiments. Advances in Water Resources 32, 750–755.

[8] Boccardo, G., Augier, F., Haroun, Y., Ferre, D., Marchisio, D.L., 2015. Validation of a novel open-source work-flow for the simulation of packed-bed reactors. Chemical Engineering Journal 279, 809–820.

[9] Boccardo, G., Crevacore, E., Passalacqua, A., Icardi, M., 2020. Computational analysis of transport in three-dimensional heterogeneous materials: An openfoam-based simulation framework. Computing and Visualization in Science 23.

[10] Boccardo, G., Sethi, R., Marchisio, D.L., 2019. Fine and ultrafine particle deposition in packed-bed catalytic reactors. Chemical Engineering Science 198, 290–304.

[11] Boccardo, G., Sokolov, I.M., Paster, A., 2018. An improved scheme for a robin boundary condition in discrete-time random walk algorithms. Journal of Computational Physics 374, 1152–1165.

[12] Carrera, J., Sánchez-Vila, X., Benet, I., Medina, A., Galarza, G., Guimerà, J., 1998. On matrix diffusion: formulations, solution methods and qualitative effects. Hydrogeology Journal 6, 178–190.

[13] Cloete, J.H., Cloete, S., Municchi, F., Radl, S., Amini, S., 2018. Development and verification of anisotropic drag closures for filtered Two Fluid Models. Chemical Engineering Science 192, 930–954. URL: https://www.sciencedirect.com/science/article/pii/S0009250918304135, doi:10.1016/J.CES.2018.06.041.

[14] Cortis, A., Gallo, C., Scher, H., Berkowitz, B., 2004. Numerical simulation of non-Fickian transport in geological formations with multiple-scale heterogeneities. Water Resour. Res 40, W04209, doi:10.1029/2003WR002750.

[15] Courant, R., Friedrichs, K., Lewy, H., 1928. Über die partiellen Differenzengleichungen der mathematischen Physik. Mathematische Annalen 100, 32–74. URL: http://link.springer.com/10.1007/BF01448839, doi:10.1007/BF01448839.

[16] Crevacore, E., Tosco, T., Sethi, R., Boccardo, G., Marchisio, D.L., 2016. Recirculation zones induce non-Fickian transport in three-dimensional periodic porous media. Physical Review E 94, 053118. URL: http://link.aps.org/doi/10.1103/PhysRevE.94.053118https://link.aps.org/doi/10.1103/PhysRevE.94.053118, doi:10.1103/PhysRevE.94.053118.

[17] Dentz, M., Berkowitz, B., 2003. Transport behavior of a passive solute in continuous time random walks and multirate mass transfer. Water Resources Research 39.

[18] Dentz, M., Cortis, A., Scher, H., Berkowitz, B., 2004. Time behavior of solute transport in heterogeneous media: transition from anomalous to normal transport. Advances in Water Resources 27, 155–173.

[19] Dentz, M., Gouze, P., Carrera, J., 2011a. Effective non-local reaction kinetics for transport in physically and chemically heterogeneous media. Journal of Contaminant Hydrology 120-121, 222–236. URL: https://doi.org/10.1016/j.jconhyd.2010.06.002, doi:10.1016/j.jconhyd.2010.06.002.

[20] Dentz, M., Icardi, M., Hidalgo, J.J., 2018. Mechanisms of dispersion in a porous medium. Journal of Fluid Mechanics 841, 851–882. URL: http://arxiv.org/abs/1709.07831https://www.cambridge.org/core/product/identifier/S0022112018001209/type/journal_article, doi:10.1017/jfm.2018.120, arXiv:1709.07831.

[21] Dentz, M., Le Borgne, T., Englert, A., Bijeljic, B., 2011b. Mixing, spreading and reaction in heterogeneous media: a brief review. J. Cont. Hydrol. 120-121, 1–17.

[22] Domenico, P.A., Schwartz, F.W. (Eds.), 1997. Physical and Chemical Hydrogeology. Wiley.

[23] Donado, L.D., Sanchez-Vila, X., Dentz, M., Carrera, J., Bolster, D., 2009. Multi-component reactive transport in multi-continuum media. Water Resour. Res. 45, W11402. doi:10.1029/2008WR006823.

[24] Driscoll, T.A., Hale, N., Trefethen, L.N., 2014. Chebfun Guide. Pafnuty Publications. URL: http://www.chebfun.org/docs/guide/.

[25] Foundation, T.O., 2014. The OpenFOAM Foundation , 4–5.

[26] Geiger, S., Dentz, M., Neuweiler, I., 2011. A Novel Multi-rate Dual-porosity Model for Improved Simulation of Fractured and Multi-porosity Reservoirs. SPE Reservoir Characterisation and Simulation Conference and Exhibition URL: http://www.onepetro.org/doi/10.2118/148130-MS, doi:10.2118/148130-MS.

[27] Georgi, A., Schierz, A., Mackenzie, K., Kopinke, F., 2015. Colloidal activated carbon for in-situ groundwater remediation—Transport characteristics and adsorption of organic compounds in water-saturated sediment columns. Journal of contaminant hydrology 179, 76–88.

[28] Gouze, P., Melean, Y., Le Borgne, T., Dentz, M., Carrera, J., 2008. Non-Fickian dispersion in porous media explained by heterogeneous microscale matrix diffusion. Water Resources Research 44.

[29] Guo, Z., Sun, Z., Zhang, N., Ding, M., Shi, S., 2019. Cfd analysis of fluid flow and particle-to-fluid heat transfer in packed bed with radial layered configuration. Chemical Engineering Science 197, 357–370.

[30] Haggerty, R., Gorelick, S.M., 1995. Multiple-Rate Mass Transfer for Modeling Diffusion and Surface Reactions in Media with Pore-Scale Heterogeneity. Water Resources Research 31, 2383–2400. URL: http://doi.wiley.com/10.1029/95WR10583, doi:10.1029/95WR10583.

[31] Haggerty, R., McKenna, S.A., Meigs, L.C., 2000. On the late-time behavior of tracer test breakthrough curves. Water Resources Research 36, 3467–3479.

[32] Herrera, I., Rodarte, L., 1973. Integrodifferential equations for systems of leaky aquifers and applications: 1. The nature of approximate theories. Water Resources Research 9, 995–1005.

[33] Herrera, I., Yates, R., 1977. Integrodifferential equations for systems of leaky aquifers and applications 3. A numerical method of unlimited applicability. Water Resources Research 13, 725–732.

[34] Horsch, M.T., Niethammer, C., Boccardo, G., Carbone, P., Chiacchiera, S., Chiricotto, M., Elliott, J.D., Lobaskin, V., Neumann, P., Schiffels, P., et al., 2019. Semantic interoperability and characterization of data provenance in computational molecular engineering. Journal of Chemical & Engineering Data .

[35] Jafari, A., Zamankhan, P., Mousavi, S., Pietarinen, K., 2008. Modeling and cfd simulation of flow behavior and dispersivity through randomly packed bed reactors. Chemical Engineering Journal 144, 476–482.

[36] Kaale, L.D., Eikevik, T.M., Rustad, T., Kolsaker, K., 2011. Superchilling of food: A review. doi:10.1016/j.jfoodeng.2011.06.004.

[37] Kekäläinen, P., Voutilainen, M., Poteri, A., Hölttä, P., Hautojärvi, A., Timonen, J., 2011. Solutions to and Validation of Matrix-Diffusion Models. Transport in Porous Media 87, 125–149. URL: http://link.springer.com/10.1007/s11242-010-9672-y, doi:10.1007/s11242-010-9672-y.

[38] Lichtner, P.C., Kang, Q., 2007. Upscaling pore-scale reactive transport equations using a multiscale continuum formulation. Water Resour. Res. 43, W12S15. doi:10.1029/2006WR005664.

[39] Liu, C., Zachara, J.M., Qafoku, N.P., Wang, Z., 2008. Scale-dependent desorption of uranium from contaminated subsurface sediments. Water Resour. Res. 44, W08413.

[40] Liu, H., Mukhopadhyay, S., Spycher, N., Kennedy, B.M., 2011. Analytical solutions of tracer transport in fractured rock associated with precipitation-dissolution reactions. Hydrogeology Journal 19, 1151.

[41] Moench, A.F., 1984. Double-Porosity Models for a Fissured Groundwater Reservoir With Fracture Skin. Water Resources Research 20, 831–846. URL: http://doi.wiley.com/10.1029/WR020i007p00831, doi:10.1029/WR020i007p00831.

[42] Moukalled, F., Mangani, L., Darwish, M., et al., 2016. The finite volume method in computational fluid dynamics. volume 113. Springer.

[43] Municchi, F., Icardi, M., 2019. Generalised Multi-Rate Models for conjugate transfer in heterogeneous materials. arXiv e-prints , arXiv:1906.01316arXiv:1906.01316.

[44] Municchi, F., Icardi, M., 2020a. Generalized multirate models for conjugate transfer in heterogeneous materials. Physical Review Research 2, 013041.

[45] Municchi, F., Icardi, M., 2020b. Macroscopic models for filtration and heterogeneous reactions in porous media. Advances in Water Resources 141, 103605. URL: https://doi.org/10.1016/j.advwatres.2020.103605https://linkinghub.elsevier.com/retrieve/pii/S0309170819308474, doi:10.1016/j.advwatres.2020.103605, arXiv:1909.02818.

[46] Municchi, F., Nagrani, P.P., Christov, I.C., 2019. A two-fluid model for numerical simulation of shear-dominated suspension flows. International Journal of Multiphase Flow 120, 103079. URL: http://arxiv.org/abs/1811.06972https://linkinghub.elsevier.com/retrieve/pii/S0301932218308899, doi:10.1016/j.ijmultiphaseflow.2019.07.015, arXiv:1811.06972.

[47] Municchi, F., Radl, S., 2017. Consistent closures for Euler-Lagrange models of bi-disperse gas-particle suspensions derived from particle-resolved direct numerical simulations. International Journal of Heat and Mass Transfer 111, 171–190. URL: http://dx.doi.org/10.1016/j.ijheatmasstransfer.2017.03.122http://linkinghub.elsevier.com/retrieve/pii/S0017931016338996, doi:10.1016/j.ijheatmasstransfer.2017.03.122.

[48] Municchi, F., Radl, S., 2018. Momentum, heat and mass transfer simulations of bounded dense mono-dispersed gas-particle systems. International Journal of Heat and Mass Transfer 120, 1146–1161. URL: https://linkinghub.elsevier.com/retrieve/pii/S0017931017338474, doi:10.1016/j.ijheatmasstransfer.2017.12.105.

[49] Municchi, F. and Di Pasquale, N. and Icardi, M. , , . mrmtfoam. URL: https://doi.org/10.5281/zenodo.3938868, doi:10.5281/zenodo.3938868.

[50] N., N., 2019. OpenFOAM: The Open Source CFD Toolbox. v1906 ed. The OpenFOAM Foundation. https://openfoam.org/.

[51] Neretnieks, I., 1980. Diffusion in the rock matrix: An important factor in radionuclide retardation? Journal of Geophysical Research: Solid Earth 85, 4379–4397.

[52] Neuman, S.P., Tartakovsky, D.M., 2009. Perspective on theories of non-Fickian transport in heterogeneous media. Advances in Water Resources 32, 670–680.

[53] Niemi, A., Bear, J., Bensabat, J. (Eds.), 2017. Geological Storage of CO2 in Deep Saline Formations. Springer Netherlands.

[54] Orgogozo, L., Golfier, F., Buès, M.A., Quintard, M., Koné, T., 2013. A dual-porosity theory for solute transport in biofilm-coated porous media. Advances in Water Resources 62, 266–279. URL: https://doi.org/10.1016/j.advwatres.2013.09.011, doi:10.1016/j.advwatres.2013.09.011.

[55] Poinssot, C., Geckeis, H. (Eds.), 2012. Radionuclide Behaviour in the Natural Environment. Woodhead Publishing.

[56] Radl, S., Municchi, F., 2018. Spatial Filtering for Scale Bridging and Its Application to Transport in Dense Particle Beds, in: Advances in Chemical Engineering. Academic Press. volume 53, pp. 153–237. URL: https://www.sciencedirect.com/science/article/pii/S0065237718300115https://linkinghub.elsevier.com/retrieve/pii/S0065237718300115, doi:10.1016/bs.ache.2018.03.001.

[57] Roth, K., Jury, W.A., 1993. Linear transport models for adsorbing solutes. Water resources research 29, 1195–1203.

[58] Silva, O., Carrera, J., Dentz, M., Kumar, S., Alcolea, A., Willmann, M., 2009. A general real-time formulation for multi-rate mass transfer problems. Hydrology and Earth System Sciences 13, 1399–1411. URL: http://www.hydrol-earth-syst-sci.net/13/1399/2009/, doi:10.5194/hess-13-1399-2009.

[59] Singhal, A., Cloete, S., Radl, S., Quinta-Ferreira, R., Amini, S., 2017. Heat transfer to a gas from densely packed beds of cylindrical particles. Chemical Engineering Science 172, 1–12. URL: https://linkinghub.elsevier.com/retrieve/pii/S0009250917303925, doi:10.1016/j.ces.2017.06.003.

[60] Song, Y., Wang, X., Yang, M., Jiang, L., Liu, Y., Dou, B., Zhao, J., Wang, S., 2013. Study of selected factors affecting hydrate-based carbon dioxide separation from simulated fuel gas in porous media. Energy & Fuels 27, 3341–3348.

[61] Sudicky, E.A., Frind, E.O., 1982. Contaminant transport in fractured porous media: Analytical solutions for a system of parallel fractures. Water Resources Research 18, 1634–1642.

[62] Tang, D., Frind, E., Sudicky, E.A., 1981. Contaminant transport in fractured porous media: Analytical solution for a single fracture. Water resources research 17, 555–564.

[63] Tecklenburg, J., Neuweiler, I., Dentz, M., Carrera, J., Geiger, S., Abramowski, C., Silva, O., 2013. A non-local two-phase flow model for immiscible displacement in highly heterogeneous porous media and its parametrization. Advances in Water Resources 62, 475–487. URL: https://doi.org/10.1016/j.advwatres.2013.05.012, doi:10.1016/j.advwatres.2013.05.012.

[64] Van Leer, B., 1974. Towards the ultimate conservative difference scheme. ii. monotonicity and conservation combined in a second-order scheme. Journal of computational physics 14, 361–370.

[65] Wang, L., Vigil, R.D., Fox, R.O., 2005. CFD simulation of shear-induced aggregation and breakage in turbulent Taylor-Couette flow. J. Colloid Interface Sci. 285, 167–178.

[66] Whitaker, S., 1986. Flow in porous media I: A theoretical derivation of Darcy's law. Transport in porous media 1, 3–25.

[67] Whitaker, S., 1999. The Method of Volume Averaging. volume 13 of *Theory and Applications of Transport in Porous Media*. Springer Netherlands, Dordrecht. URL: http://books.google.com/books?hl=fr&lr=&id=x7mQCEokSCAC&pgis=1http://link.springer.com/10.1007/978-94-017-3389-2, doi:10.1007/978-94-017-3389-2.

[68] Yan, W., Lien, H., Koel, B.E., Zhang, W., 2013. Iron nanoparticles for environmental clean-up: recent developments and future outlook. Environmental Science: Processes & Impacts 15, 63–77.

[69] Zhou, J., Wang, L., Chen, Y., Cardenas, M.B., 2019. Mass Transfer Between Recirculation and Main Flow Zones: Is Physically Based Parameterization Possible? Water Resources Research 55, 345–362. URL: https://onlinelibrary.wiley.com/doi/abs/10.1029/2018WR023124, doi:10.1029/2018WR023124.

[70] Zou, L., Jing, L., Cvetkovic, V., 2017. Modeling of solute transport in a 3D rough-walled fracture–matrix system. Transport in Porous Media 116, 1005–1029.